


## Article

# The Early Age Hydration Products and Mechanical Properties of Cement Paste Containing GBFS under Steam Curing Condition

Baoliang Li <sup>1,\*</sup> , Zhouyang Tang <sup>1</sup>, Binbin Huo <sup>2</sup>, Zejun Liu <sup>1</sup>, Yongzhen Cheng <sup>1</sup>, Baizhan Ding <sup>3</sup> and Peng Zhang <sup>1,\*</sup>

<sup>1</sup> Faculty of Architecture and Civil Engineering, Huaiyin Institute of Technology, Huaian 223001, China

<sup>2</sup> State Key Laboratory of Coal Resources and Safe Mining, School of Mines, China University of Mining and Technology, Xuzhou 221116, China

<sup>3</sup> Huaian Construction Engineering Quality Testing Center Co., Ltd., Huaian 223003, China

\* Correspondence: lbjndx@126.com (B.L.); zhangpeng87@hyit.edu.cn (P.Z.)

**Abstract:** The hydration products and strength of cement pastes incorporated with ground blast furnace slag (GBFS) (0% and 20% replacement) have been investigated under steam curing condition (80 °C for 7 h and 7 d) in comparison with normal curing condition (moist curing for 28 d). The results show that, during the initial 80 °C steam curing for 7 h, in addition to the filler effect, GBFS is still involved in cement hydration. The abundant available Al phase and Mg phase in GBFS promote the formation of flake-like hydrotalcite, foil-like C-(A)-S-H gels, as well as equant grain-shaped C-(A)-S-H gels. Prolonging the steam curing time to 7 d further improves the formation of hydrogarnet. Since the formation of both hydrogarnet and hydrotalcite can consume the available Al, steam curing for 7 d seems to favor the formation of low Al C-(A)-S-H gels. In addition, due to the formation of a large amount of hydration products, the influence of 20% GBFS addition on the demolding strength of initial steam-cured cement mortar (80 °C for 7 h) is almost negligible. However, further extending the steam curing time to 7 d increases the strength gap between 20% GBFS blended cement mortar and pure cement mortar, and the related mechanism is discussed.

**Keywords:** GBFS; steam curing; hydration products; strength



**Citation:** Li, B.; Tang, Z.; Huo, B.; Liu, Z.; Cheng, Y.; Ding, B.; Zhang, P. The Early Age Hydration Products and Mechanical Properties of Cement Paste Containing GBFS under Steam Curing Condition. *Buildings* **2022**, *12*, 1746. <https://doi.org/10.3390/buildings12101746>

Academic Editor: Lukasz Sadowski

Received: 2 September 2022

Accepted: 18 October 2022

Published: 20 October 2022

**Publisher's Note:** MDPI stays neutral with regard to jurisdictional claims in published maps and institutional affiliations.



**Copyright:** © 2022 by the authors. Licensee MDPI, Basel, Switzerland. This article is an open access article distributed under the terms and conditions of the Creative Commons Attribution (CC BY) license (<https://creativecommons.org/licenses/by/4.0/>).

## 1. Introduction

Prefabricated concrete elements have attracted more attention due to their advantages of shortening construction time, reducing construction cost, and improving the construction quality of buildings [1], and are widely used in cross-sea bridges and municipal engineering. Currently, they account for around 20% of the world's total concrete production. In order to shorten the manufacturing cycle and improve the early strength of prefabricated concrete elements, steam curing is one of the common measures adopted [1,2]. Although steam curing accelerates the early hydration of cement, the “Hot Damage Effect (HDE)” triggered by thermal treatment will cause heterogeneous distribution of hydration products and form more micro-cracks and pores, resulting in higher permeability which is detrimental to the durability of concrete [3–5].

To alleviate the adverse effects of HDE and improve the durability of prefabricated components, previous studies have focused on improving steam curing regime and the use of supplementary cementitious material (SCM) to replace portions of cement. Typical steam curing regime is generally composed of a pre-curing period, heating period, constant temperature curing period, as well as the following cooling period [6]. It is reported that prolonging the time in the pre-curing period, slowing down the heating rate in the heating period, reducing the temperature in the constant temperature curing period, and adopting a lower cooling rate, have been proved to be effective in reducing the adverse effects brought on by steam curing [6–8]. In addition, it should be noted that subsequent curing also plays an important role in the performance development of steam-cured concrete, and a

positive correlation between adequate subsequent curing and better macro-performance has been found. Liu et al. [9] investigated that, in comparison with subsequent air curing, subsequent wet curing (including moist curing, water curing, as well as saturated lime water curing) is competitive in improving the pore structure of steam cured concrete, and the longer the subsequent wet curing time, the more effective it is to improve the durability of steam-cured concrete to a certain extent. In the process of steam curing, the covering measures of the concrete surface are also very important to the durability of concrete. Shi et al. [6] found that since a geotextile can use adsorbed water to replenish the concrete when the concrete is short of water, the concrete covered with a geotextile is denser than that covered with plastic film.

With the improvement of steam curing regimes, the role of SCM in improving the durability of steam-cured concrete has attracted a growing concern. Escalante-Garcia et al. [10] revealed that the raised temperature reduces the hydration degree of neat cement in the longer term; however, the presence of SCM is expected to change its hydration patterns. Wang et al. [11] indicated that fly ash (FA) addition lowers not only the drying shrinkage, but also the autogenous shrinkage of steam-cured concrete. Chen et al. [12] revealed that adding both metakaolin and limestone powder can reduce the sorptivity and improve the mechanical properties of the steam-cured concrete. Liu et al. [13] presented that in comparison with steam curing 80 °C for 8 h, steam curing 60 °C for 11 h can help concrete incorporated with phosphorus slag gain an ideal demolding strength and chloride permeability. The authors' investigation showed that adding lithium slag can improve demolding strength, ferronickel slag incorporation can promote the late strength, while steel slag addition is detrimental to the strength of steam-cured concrete [14–16]. Although these three SCMs have little influence on hydration products, they can improve the sulfate resistance of steam-cured concrete. However, compared with the SCMs mentioned above, ground blast furnace slag (GBFS) is the most widely used in prefabricated components at present [17–19].

The abundant amorphous phases endow GBFS with high pozzolanic reactivity, which is helpful to repair the thermal damage and compensate for strength loss caused by elevated temperature curing [20]. Escalante-Garcia et al. [10] reported that the presence of GBFS accelerates the hydration of alite from very early stages. A lower CH content appeared in 60 °C cured GBFS blended cement paste compared to that cured at normal curing suggested that the elevated temperature favors the pozzolanic reaction of GBFS in the early stages of hydration. Barnett et al. [21] implied that the early age strength of mortar blended with high level GBFS is much more sensitive to temperature; even a 10 °C increase can considerably enhance the mortar strength, so that its strength gained at 40~50 °C is basically equivalent to that pure cement mortar after 3 days. Yu et al. [22] found that the combination of GBFS and FA not only reduced the temperature difference between inside and outside of the specimen, but also lessened the concrete expansion caused by steam curing. Zhuang et al. [23] noted that large amounts of ultrafine slag contribute to better demolding strength, higher sulfate resistance, as well as lower permeability of steam-cured concrete.

Although GBFS addition can improve the durability of steam-cured concrete, the effect of GBFS on the early properties of steam-cured concrete, especially the early hydration products and mechanical properties, is still unclear. Generally, precast concrete is used immediately after demolding; therefore, the effect of GBFS on early age hydration products and mechanical properties is very important to understand the action mechanism of GBFS in steam-cured concrete.

GBFS contains around 10.6~15.1%  $\text{Al}_2\text{O}_3$  and 8.0~9.4%  $\text{MgO}$  [1,20–23]. How such a large amount of  $\text{Al}_2\text{O}_3$  and  $\text{MgO}$  affect the hydration products and microstructure of concrete during steam curing is rarely reported. Therefore, the hydration product composition and mechanical properties of GBFS-incorporated cement paste were studied under the conditions of steam curing (80 °C for 7 h and 7 d) compared with that of normal curing (standard curing for 28 d). This investigation revealed that the GBFS

addition promoted the uptake of Al by C-S-H gels and the formation of hydrotalcite at elevated temperatures, and that the extension of steam curing time would further promote the production of hydrogarnet. These results are helpful for understanding the action mechanism of GBFS in steam-cured concrete.

## 2. Materials and Methods

### 2.1. Raw Materials

The cement used was PII52.5 Portland cement (PC) with loss-on-ignition (LOI) of 2.4% and specific surface area of 356 m<sup>2</sup>/kg. Type S95 GBFS with LOI of 2.1% and specific surface area of 536 m<sup>2</sup>/kg was used. The chemical compositions of PC and GBFS tested by XRF are shown in Table 1. The particle size distribution curves of cement and GBFS determined by a Microtrac S3500 laser particle size analyzer are shown in Figure 1. The maximum particle size of GBFS was 44.7 μm, and the average particle size was 6.34 μm, which was much smaller than the corresponding value (422.2 μm and 16.1 μm) in PC.

**Table 1.** Chemical composition of PC and GBFS, wt.%.

Oxide	CaO	SiO <sub>2</sub>	Al <sub>2</sub> O <sub>3</sub>	SO <sub>3</sub>	Fe <sub>2</sub> O <sub>3</sub>	MgO	Na <sub>2</sub> O	K <sub>2</sub> O
PC	64.47	20.87	4.87	2.52	3.59	2.13	0.11	0.65
GBFS	44.40	29.56	14.87	2.98	0.40	6.72	-	0.49

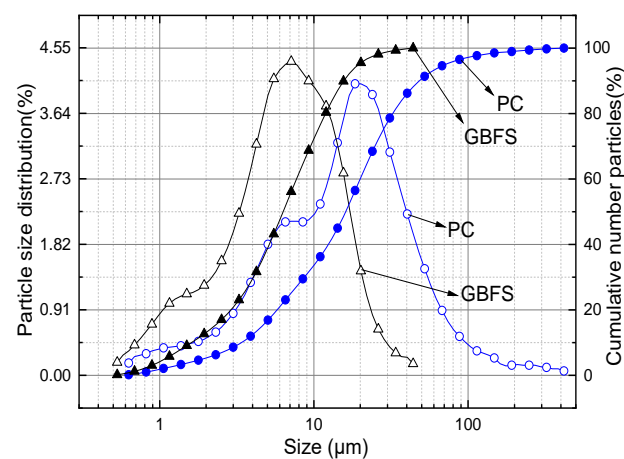


**Figure 1.** Particle size distribution of PC and GBFS.

The XRD analysis of the GBFS is shown in Figure 2. The GBFS was mainly composed of amorphous phase, which is responsible for its latent hydraulic or pozzolanic reactivity. Generally, the average amount of glassy phase in GBFS is often above 90% [24]; thus, the reactivity of GBFS was higher than other SCM. The 28 d strength activity index of GBFS used in this investigation reached 103%, which meets the requirements of Type S95 GBFS.

### 2.2. Sample Preparation and Test Methods

Previous studies have shown that the optimal substitution level of GBFS in cement is 10–20% [25]; therefore, 0% and 20% replacement were considered in this investigation. Under the condition of water-binder ratio of 0.3 [26], the cement paste was prepared according to the mix proportion in Table 2. In order to simulate the actual curing regime on site and activate the reactivity of GBFS, 80 °C steam curing for 7 h (S7h, steam curing at constant 80 °C for 7 h), and 80 °C steam curing for 7 d (S7d, steam curing at constant 80 °C for 7 d) were adopted in comparison with the condition of standard curing for 28 d (N28d, cured at 20 ± 2 °C, and relative humidity larger than 95% for 28 d). The corresponding steam curing regime can be referred to in Figure 3. The hydration of specimens at corresponding ages was terminated with anhydrous ethanol, then dried at 60 °C for 24 h in a vacuum-drying

oven. Subsequently, the composition of hydration products in the cement paste containing GBFS were determined by XRD, SEM-EDS, and TG-DTG.

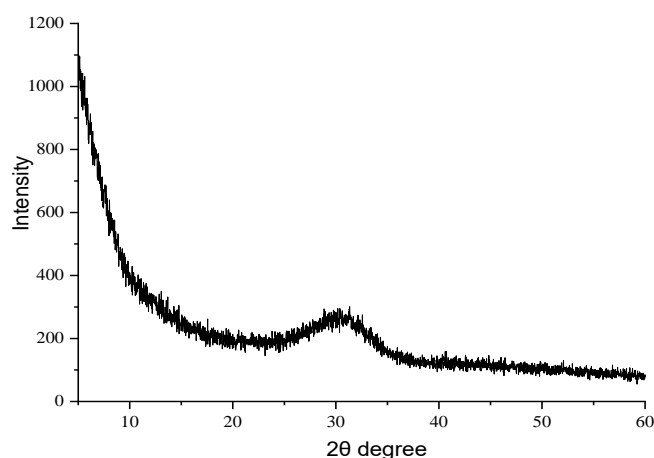


Figure 2. XRD result of GBFS.

Table 2. Mix proportion (wt. %) and physical properties of GBFS blended cement.

Sample	PC	GBFS	Water Demand (wt. %)	Setting Times (h: min)	
				Initial	Final
Ref	100	0	27.4	2:52	3:57
G20	80	20	28.0	2:45	3:32

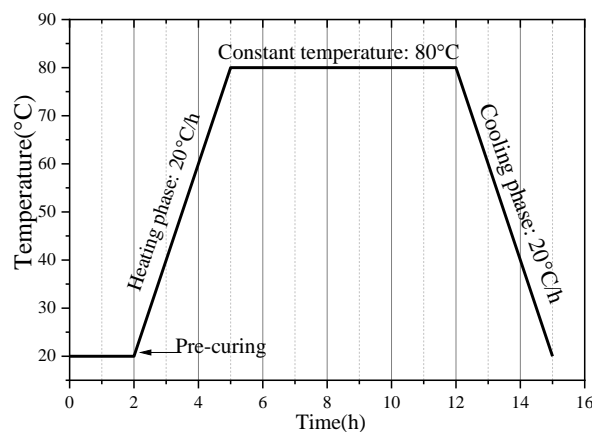


Figure 3. The regime for steam curing.

According to the mix proportion in Table 2, mortars with the same curing condition were prepared (binder: water: standard sand = 1:0.5:3). The mechanical properties of cement mortar were carried out according to Chinese standard GB/T 17671-1999. For steam-cured samples, mechanical properties were tested after demolding, whereas strength tests for standard cured samples were performed after 28 d of moist curing. The basic physical properties of PC and GBFS blended cement are also shown in Table 2, in which the shorter setting time of G20 is related to the larger specific surface area and the higher content of  $\text{SO}_3$  in GBFS.

XRD test: the composition of GBFS and the hydration products in hardened cement paste were checked using a D8-Discover X-ray diffractometer (XRD) using  $\text{CuK}\alpha 1$  radiation, 40 kV voltage, and 36 mA current with the scanning speed of  $3^\circ/\text{min}$ .

SEM-EDS test: the fresh and dry fracture surfaces of mortars were observed using a Sirion (FEI) field emission scanning electron microscope (SEM), and the related composi-

tions were checked by energy dispersive X-ray spectra (EDS). It is worth noting that the samples were dried and sprayed with gold before the SEM-EDS test.

TG-DTG test: STA 449 F3 Jupiter<sup>®</sup> was used to carry out TG/DTG by heating cement paste from room temperature to 1000 °C at 10 °C/min under nitrogen atmosphere.

### 3. Results

#### 3.1. XRD Analysis of Hydration Products

Figure 4 shows the XRD patterns of the hydration products of pure cement paste and composite cement paste blended with 20% GBFS, under steam curing condition and 28 d standard curing condition.

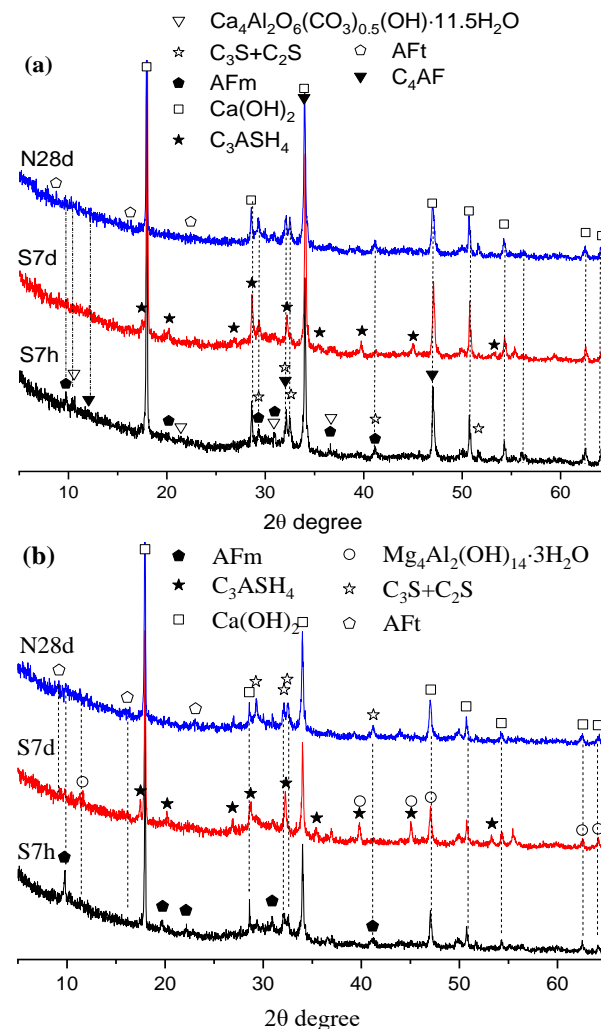


**Figure 4.** XRD of cement pastes under various curing conditions (a) Ref; (b) G20.

In addition to the C-S-H gels, the hydration products of pure cement paste (Figure 4a) under the condition of steam curing for 7 h included  $\text{Ca}(\text{OH})_2$ , monosulfoaluminate hydrate (AFm), and semi-carbonate ( $\text{Ca}_4\text{Al}_2\text{O}_6(\text{CO}_3)_{0.5}(\text{OH})\cdot 11.5\text{H}_2\text{O}$ ). Different from steam curing for 7 h, hydrogarnet ( $\text{C}_3\text{ASH}_4$ ) was formed in pure cement paste under steam curing for 7 d, while ettringite (AFt) was formed under standard curing for 28 d. Since AFt is unstable at elevated temperatures, there is no AFt produced under steam curing. Limestone powder is a common filler for cement, and consequently, the formation of semi-carbonates was found in pure cement paste, regardless of curing conditions.

From Figure 4b, it can be seen that the main hydration products of blended cement paste incorporated with GBFS were C-S-H gel, CH, AFt, AFm, and  $\text{Mg}_4\text{Al}_2(\text{OH})_{14}\cdot 3\text{H}_2\text{O}$  (hydrotalcite) at normal curing for 28 d, which is consistent with the study of Chen et al. [27].

Apart from C-S-H gels, the hydration products of S7h G20 also presented CH, AFm, and hydrotalcite. When the steam curing time was extended to 7 d, hydrogarnet appeared too. Nonetheless, AFt is unstable and will convert into AFm at 80 °C, the traces of AFt were still observed, which may be related to the high SO<sub>3</sub> content in GBFS [14].

The reactivity of GBFS principally depends on its source, chemical composition, pre-treatment process (e.g., the content of amorphous phases, structure, cooling rate, particle size, etc.), and the pore solution of hardened cement paste [28]. In addition, it also depends on the curing temperature and the replacement level of GBFS. Under the conditions of higher curing temperature (>50 °C) and lower substitution ratio (<20%), cement paste can release a large amount of Ca(OH)<sub>2</sub>, under such a high temperature and high alkali environment, GBFS dissolves quickly and has a high reactivity [29]. In this investigation, the more amorphous phase and higher specific surface area ensured the higher reactivity of GBFS under 80 °C steam curing [30]. In particular, GBFS contains a high content of reactive Al and Mg phases, which can affect the composition and type of hydration products; in consequence, hydrotalcite is generated under the condition of steam curing. It has been reported that hydrotalcite has a good chloride ion binding ability [31]. Moreover, the formation of hydrotalcite consumes the available Al that should be involved in AFm precipitation; thus, it reduces the content of AFm which can react with the intruded sulfate, and thereby improves the sulfate resistance [32].

Hydrogarnet (C<sub>3</sub>AH<sub>6</sub>) is transformed from metastable phases CAH<sub>10</sub>, C<sub>2</sub>AH<sub>8</sub>, and C<sub>4</sub>AH<sub>13</sub>. This conversion rate is positively correlated with temperature: this conversion rate is slow at 5 °C, and very fast at temperatures above 50 °C. This transformation will lead to the decrease of solid volume and the increase of porosity [33]; therefore, the formation of hydrogarnet will result in the loss of late strength of high-aluminate cement or high-temperature cured concrete. It is worth noting that, due to the high content of SiO<sub>2</sub> in cement and the use of Si-rich SCMs, hydrogarnet in cement and concrete often exists in the form of C<sub>3</sub>ASH<sub>4</sub>, and its chemical formula is between C<sub>3</sub>AH<sub>6</sub>~C<sub>3</sub>AS<sub>3</sub> [34]. Based on this, in order to avoid the formation of hydrogarnet phase, high-aluminate cement is often mixed with Si-rich additives, such as 40~60% GBFS or 17~20% natural zeolite [35], so that the C<sub>2</sub>ASH<sub>8</sub> phase is preferred to form instead of hydrogarnet, thus avoiding the reduction of strength. At the same time, increasing the ratio of metakaolin to cement or the ratio of reactive Si to reactive Al in composite cement at room temperature is also conducive to the generation of C<sub>2</sub>ASH<sub>8</sub> phase instead of C<sub>4</sub>AH<sub>13</sub>, thus inhibiting the transformation of C<sub>4</sub>AH<sub>13</sub> to hydrogarnet [36]. Nevertheless, whether increasing GBFS content can avoid or reduce the formation of hydrogarnet in blended cement under long-term high temperature curing needs further investigation.

### 3.2. Morphology and Composition of Hydration Products Determined by SEM-EDS

#### 3.2.1. Hydration Products under 80 °C Steam Curing for 7 h

The hydration products of pure cement paste and composite cement paste mixed with 20% GBFS under the condition of steam curing for 7 h are shown in Figures 5 and 6, respectively. As can be seen from Figure 5, the hydration products of steam-cured 7 h pure cement paste were mainly loose fibrous C-S-H gels (Figure 5a), flake CH (Figure 5c), accompanied by many pores (Figure 5a,c).

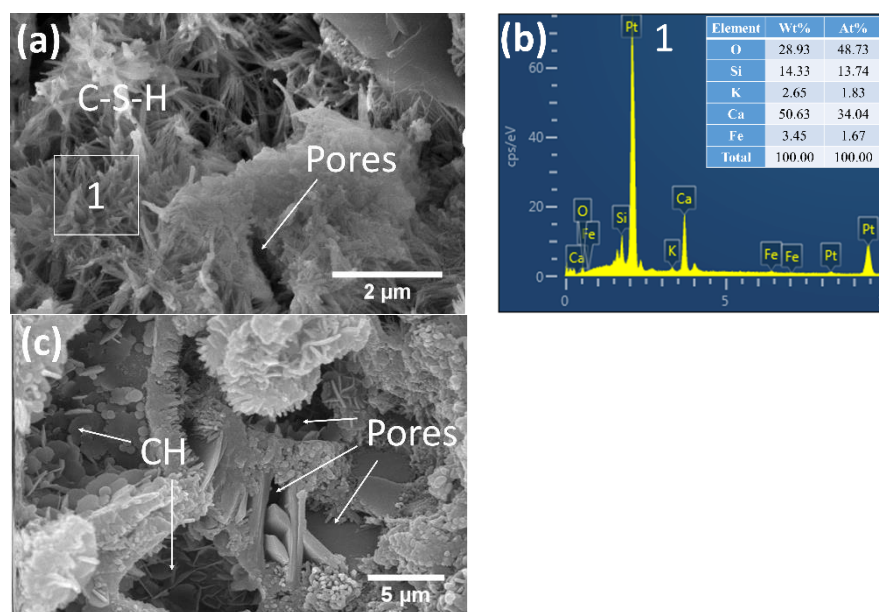


**Figure 5.** SEM images of pure cement paste after 80 °C steam curing for 7 h, (a) fibrous C-S-H gels; (b) EDS result of area 1; (c) pores. Note: Wt% represents the mass percentage, At% represents the atomic percentage.

As shown in Figure 6, in addition to fibrous C-S-H gels (Figure 6a), foil-like and equant grain-shaped C-S-H gels also appeared in cement-GBFS composite binder (Figure 6c). As can be seen from Figure 6d, the presence of Al and Mg have influenced the formation of C-S-H gels, which are considered to be responsible for the morphology change of C-S-H gels. In addition, flake-like hydration products (Figure 6e) were produced. According to its EDS result (Figure 6f), it contains high contents of Mg and Al, and its Mg/Al ratio is 1.67, close to 2; accordingly, it can be speculated that it is hydrotalcite ( $\text{Mg}_4\text{Al}_2(\text{OH})_{14}\cdot 3\text{H}_2\text{O}$ ), which can be confirmed by the XRD results shown in Figure 4b. However, due to the short hydration time, there are still many pores in the GBFS-cement composite binder, as shown in Figure 6g.

Under the condition of 80 °C steam curing, a large amount of  $\text{OH}^-$  released by cement hydration can quickly invade into the network structure of amorphous phase in GBFS, dissolve  $\text{Ca}^{2+}$  and  $\text{Mg}^{2+}$  in the Ca-rich phase, and interact with  $\text{Si}^{4+}$  and  $\text{Al}^{3+}$  in the Si-rich phase, and thereby form C-S-H and C-A-H [37]. Additionally, in comparison with C-S-H gels in pure cement paste (Figure 5b), the uptake of Al in C-S-H gels in GBFS-blended cement paste is more evident and has been reported [38], which suggested that the C-(A)-S-H gels formation is easier in GBFS-blended cement under steam curing. Although the trace of Mg was also found in the EDS results (Figure 6b,d), it was still difficult to prove the uptake of Mg by C-S-H gels due to the different structure between M-S-H and C-S-H gels [38], and further study is needed to determine the role of Mg in the C-S-H gels formation. Moreover, according to the EDS results in S7h (Figures 5b and 6b,d), the Ca/Si ratio of C-S-H gels was around 2.17~2.49, indicating that the hydration degree of cement paste after steam curing for 7 h was relatively high, which is related to the accelerated cement hydration at steam curing.

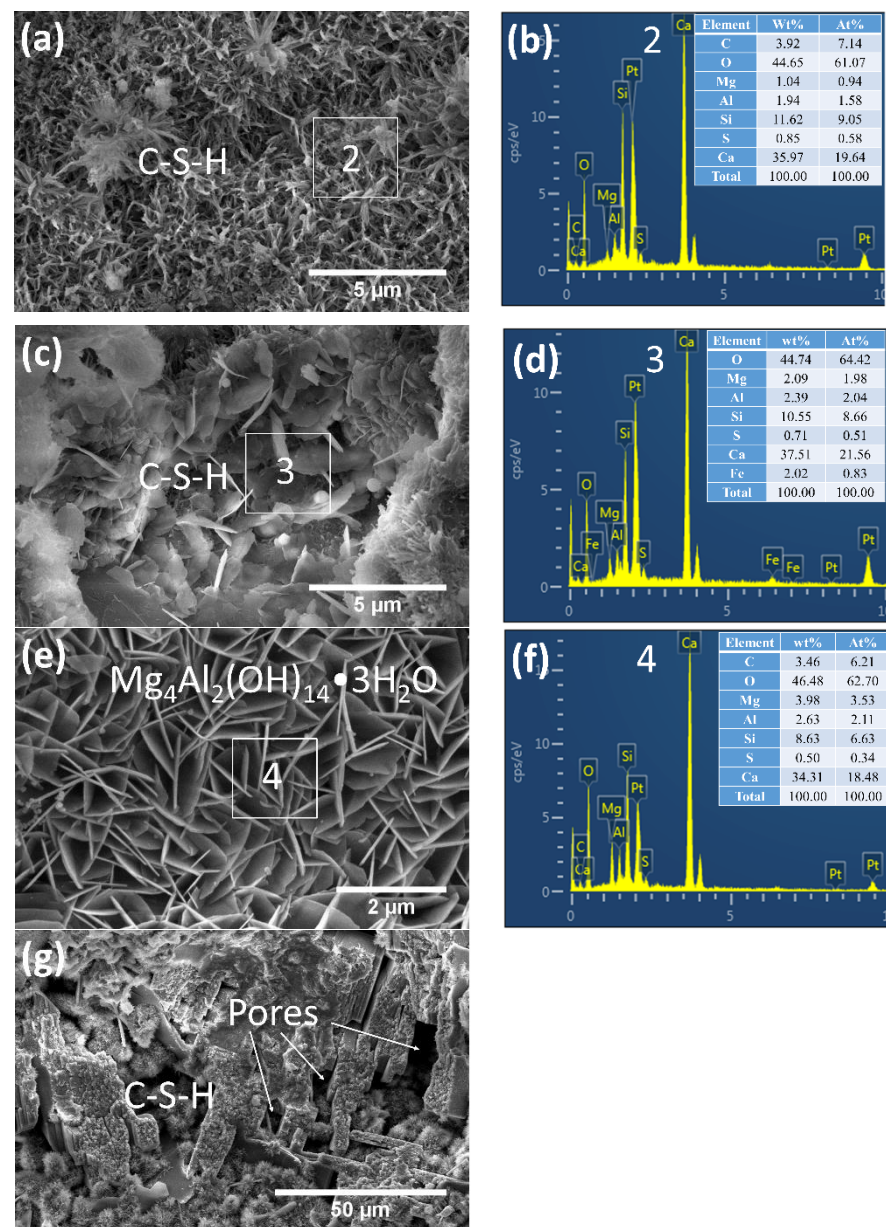


**Figure 6.** SEM images of cement-GBFS composite binder after 80 °C steam curing for 7 h, (a) fibrous C-S-H gels; (b) EDS result of area 2; (c) foil-like and equant grain-shaped C-S-H gels; (d) EDS result of area 3; (e) flake-like hydrotalcite; (f) EDS result of area 4; (g) pores.

### 3.2.2. Hydration Products under 80 °C Steam Curing for 7 d

The hydration products of pure cement paste and cement-GBFS composite binder under steam curing for 7 days are shown in Figures 7 and 8, separately. The hydration products of pure cement paste were mainly fibrous C-S-H gels (Figure 7a) and flake CH (Figure 7c), and obvious cracks occurred after a long time of steam curing (Figure 7c). In addition, the hydration products of spherical particles with the approximate size of 1 μm were generated, as shown in Figure 7c. Combined with the morphology [39] and the XRD results in Figure 4a, it can be confirmed that it is hydrogarnet.



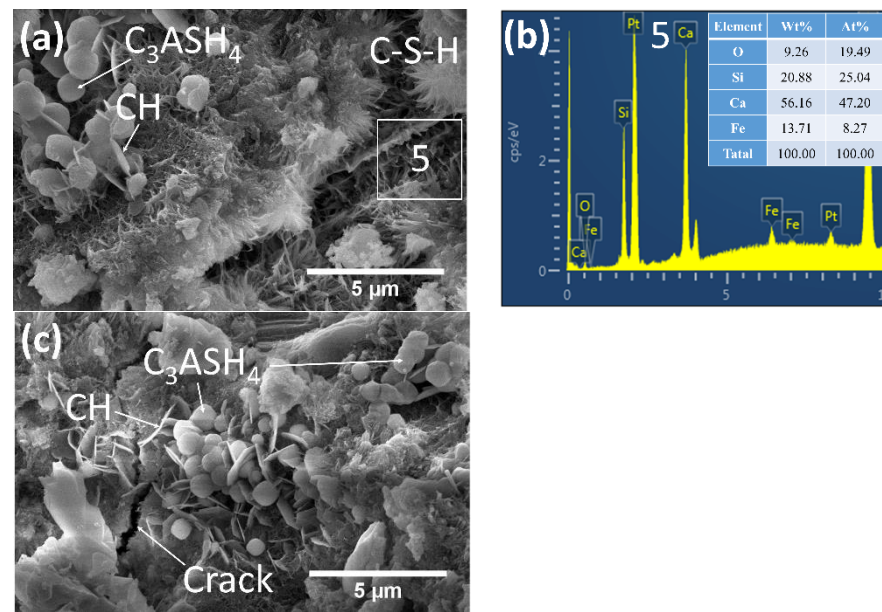


**Figure 7.** SEM images of pure cement paste after 80 °C steam curing for 7 d, (a) fibrous C-S-H gels; (b) EDS result of area 5; (c) spherical hydrogarnet and crack.

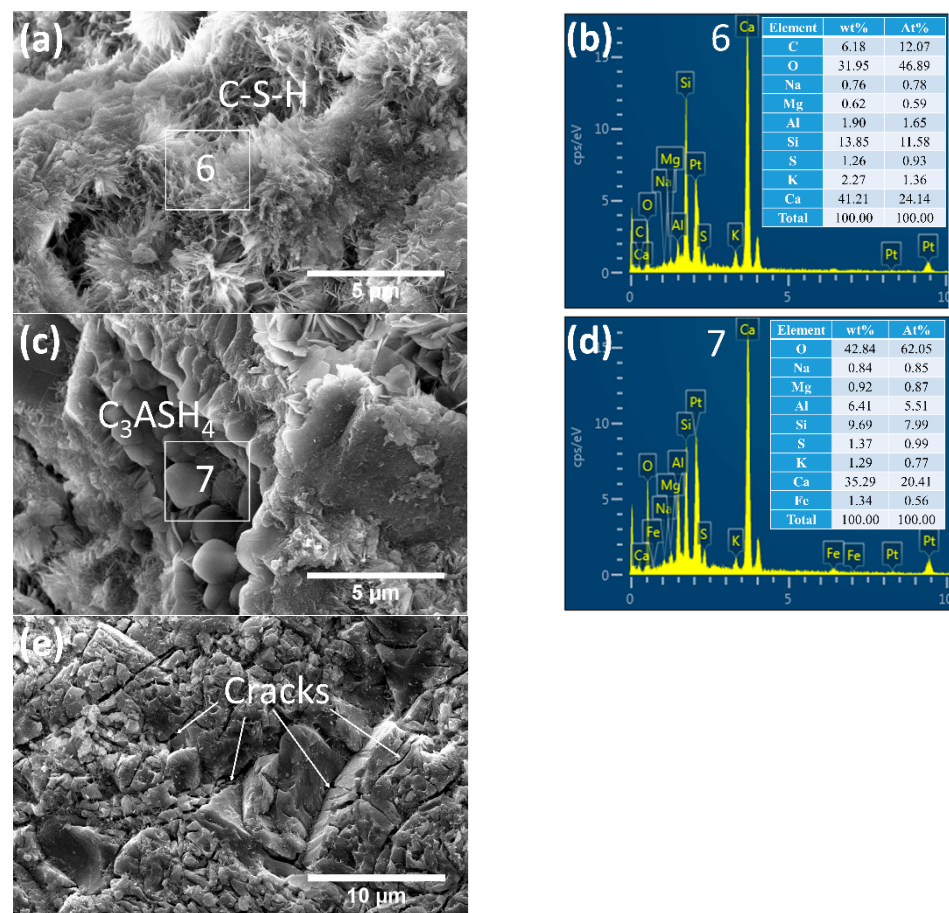


**Figure 8.** SEM images of cement-GBFS composite binder after 80 °C steam curing for 7 d, (a) fibrous C-S-H gels; (b) EDS result of area 6; (c) spherical hydrogarnet; (d) EDS result of area 7; (e) cracks.

The morphology of C-S-H gels in S7d G20 was mainly fibrous (Figure 8a). In addition, 1–2  $\mu m$  granular hydration products (Figure 8c) appeared, whose Ca/Al ratio (3.70) and

Al/Si ratio (0.69) (Figure 8d) were close to the proportion of each element in  $C_3ASH_4$ . Consequently, combined with the results shown in Figure 4, it can be determined as hydrogarnet. However, it should be noted that the particle size of hydrogarnet in S7d G20 is larger than that in S7d Ref (1  $\mu\text{m}$ ), which may be related to the sufficient available Al in GBFS. At the same time, more obvious cracks in S7d G20 appeared, as shown in Figure 8e. In addition to long-term high temperature steam curing, whether it is also related to the production of more hydrogarnet needs to be further studied. Although steam curing is helpful for the uptake of Al by C-S-H gels, the prolongation of steam curing time seems to be more conducive to the formation of low-Al C-(A)-S-H gels (lower Al/Si ratio of C-(A)-S-H in Figure 6b,d compared to that in Figure 8b) which is attributed to more available Al participation in the formation of hydrotalcite and hydrogarnet at this time [40]. Furthermore, according to the EDS results in S7d (Figures 7b and 8b), the Ca/Si ratio of C-S-H gels was around 1.88~2.08, lower than that in S7h, indicating that the hydration degree of cement paste under S7d is higher than S7h, which is undoubtedly related to the prolonged steam curing time. Generally, the average polymerization degree of C-S-H gels increases when its Ca/Si ratio decreases [41], and at the same time, the compressive strength of the C-S-H paste also increases [42].

### 3.2.3. Hydration Products under 28 d Standard Curing

Hydration products of pure cement paste and cement-GBFS composite binder are shown in Figures 9 and 10, respectively. More hydration products (Figure 9a) appeared in pure cement paste after 28 d normal curing, and the C-S-H gel interwoven with CH made the structure relatively compact (Figure 9b).

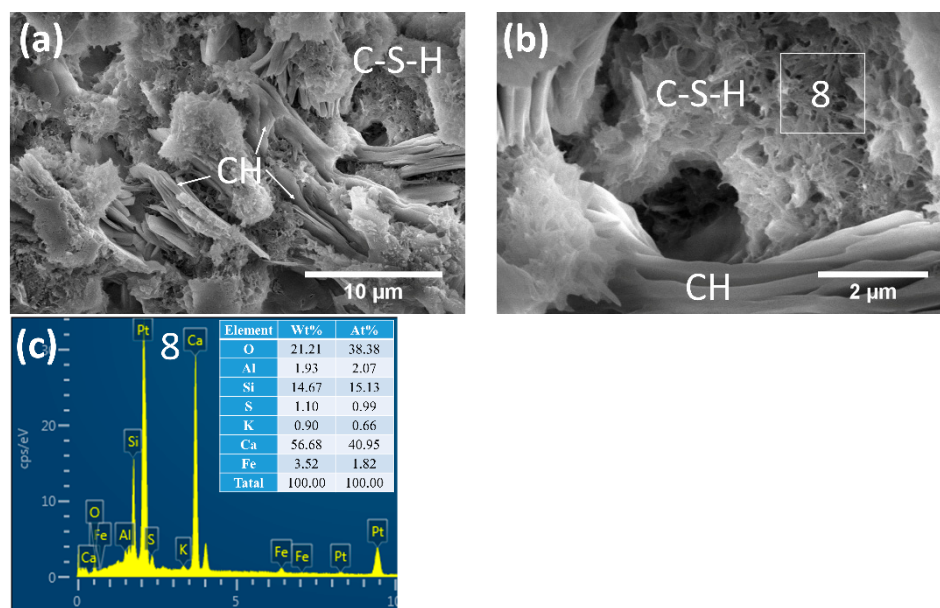


**Figure 9.** SEM images of pure cement paste after standard curing for 28 d, (a) reticular C-S-H gels and CH; (b) reticular C-S-H gels and CH; (c) EDS result of area 8.

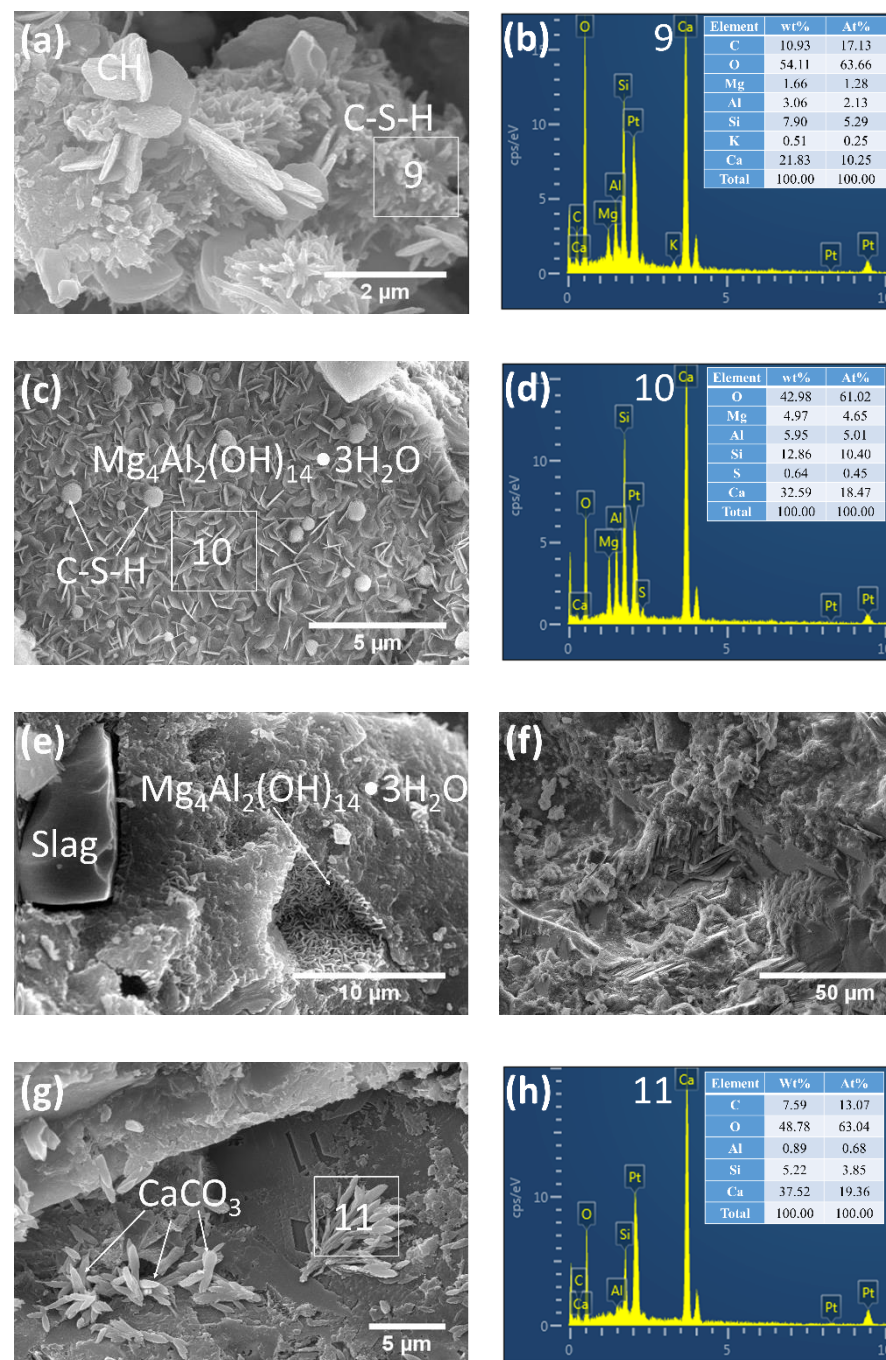


**Figure 10.** SEM images of cement-GBFS composite binder after standard curing for 28 d, (a) fibrous C-S-H gels; (b) EDS result of area 9; (c) flake-like hydrotalcite and quant grain-shaped C-S-H gels; (d) EDS result of area 10; (e) flake-like hydrotalcite; (f) dense microstructure; (g) tadpole-like  $\text{CaCO}_3$ ; (h) EDS result of area 11.

Different from C-S-H gels in pure cement paste, fibrous and equant grain-shaped C-S-H (Figure 10a,c) and CH with smaller particle size (Figure 10a) appeared in standard-cured GBFS-blended cement paste. Furthermore, flake-like hydrotalcite was observed in Figure 10c,e, which agrees with the above XRD results. In accordance with the research of most studies, adding mineral powder can reduce the porosity of concrete and densify its microstructure (Figure 10f). It is interesting to note that tadpole-like and fibrous products also were produced in GBFS-mixed cement paste (Figure 10g). It can be seen from Figure 10h that this product was mainly composed of C, Ca, and O; thus, it can be

determined as  $\text{CaCO}_3$ . The formation of tadpole-like  $\text{CaCO}_3$  may be related to the use of anhydrous ethanol to terminate the hydration of the sample in this investigation [43]. It is well known that  $\text{CaCO}_3$  usually has three types of structures: calcite, aragonite, and vaterite, with cubic, spherical, fibrous, flake, and petal-like morphologies, etc. [43]. The morphology of  $\text{CaCO}_3$  is mainly affected by the pH value, foreign ions ( $\text{Mg}^{2+}$ , etc.), organic additives (alcohols, acids, amino acids, proteins, and sugars), and the supersaturation degree of the solution [43], of which alcohol additives mainly affect the morphology of  $\text{CaCO}_3$  by affecting the dielectric constant of the medium, the attraction between ions and the interaction between solute and solvent [43].

Furthermore, according to the EDS results in N28d (Figures 9c and 10b), the Ca/Si ratio of C-S-H gels was around 1.94~2.71, which is similar to that in S7h, but lower than that in S7d, indicating that the hydration degree of cement paste in N28d is similar to that of S7h, but slightly lower than that of S7d.

### 3.3. Hydration Products Determined by TG/DTG Analysis

Figure 11 shows the TG/DTG curve of pure cement paste and GBFS-blended cement pastes under different curing conditions. As can be seen from Figure 11, under the conditions of S7h and N28d, the type of hydration products in Ref and G20 are basically the same. In comparison with the condition of S7h and N28d, the weight loss of pure cement paste at 300~390 °C under the condition of S7d is more obvious (Figure 11a), and it is reported that the weight loss between this interval is mainly caused by the decomposition of hydrogarnet [44], which closely matches the above XRD and SEM results. However, compared with Ref, the weight loss in G20 at 300~390 °C is more significant, which is related to the formation of hydrotalcite in addition to the hydrogarnet generation in G20 under S7d curing conditions. Furthermore, it can be seen that, due to the high  $\text{SO}_3$  content in GBFS, there is still a small amount of ettringite in the steam-cured GBFS-mixed cement pastes.

The non-evaporable water and CH content of Ref and G20, calculated by using the mass loss of samples in specific temperature ranges in Figure 11, are tabulated in Table 3 [14]. Under the conditions of S7h and N28d, the non-evaporable water and CH content of G20 were basically the same, indicating that early steam curing promoted the reaction between cement and GBFS, which made its hydration degree equal to that of standard-cured for 28 d.

**Table 3.** Total mass loss, non-evaporable water, and CH content of cement pastes, wt.%.

Samples		Mass Loss	Non-Evaporable Water	CH
Ref	S7h	18.43	20.13	19.34
	S7d	20.75	23.72	24.07
	N28d	20.73	23.69	20.00
G20	S7h	19.29	21.52	13.40
	S7d	21.45	24.93	18.74
	N28d	19.26	21.47	13.29

In addition, under the conditions of S7h, S7d, and N28d, the non-evaporable water of G20 reached 106.9%, 105.1%, and 90.6% that of Ref, respectively, revealing that GBFS addition promotes the hydration of steam-cured pure cement paste, which is related to both the high content of  $\text{SO}_3$  and the high activity of GBFS [45]. Under the above three curing conditions, the CH content of G20 was 69.3%, 77.9%, and 66.5% that of Ref, respectively. It suggests that GBFS participates in the cement hydration and consumes CH under steam curing condition, especially at steam curing for 7 h; however, prolonging the steam curing time from 7 h to 7 d is not conducive to the further reduction in the ratio of CH content in G20 to that in Ref (77.9%).

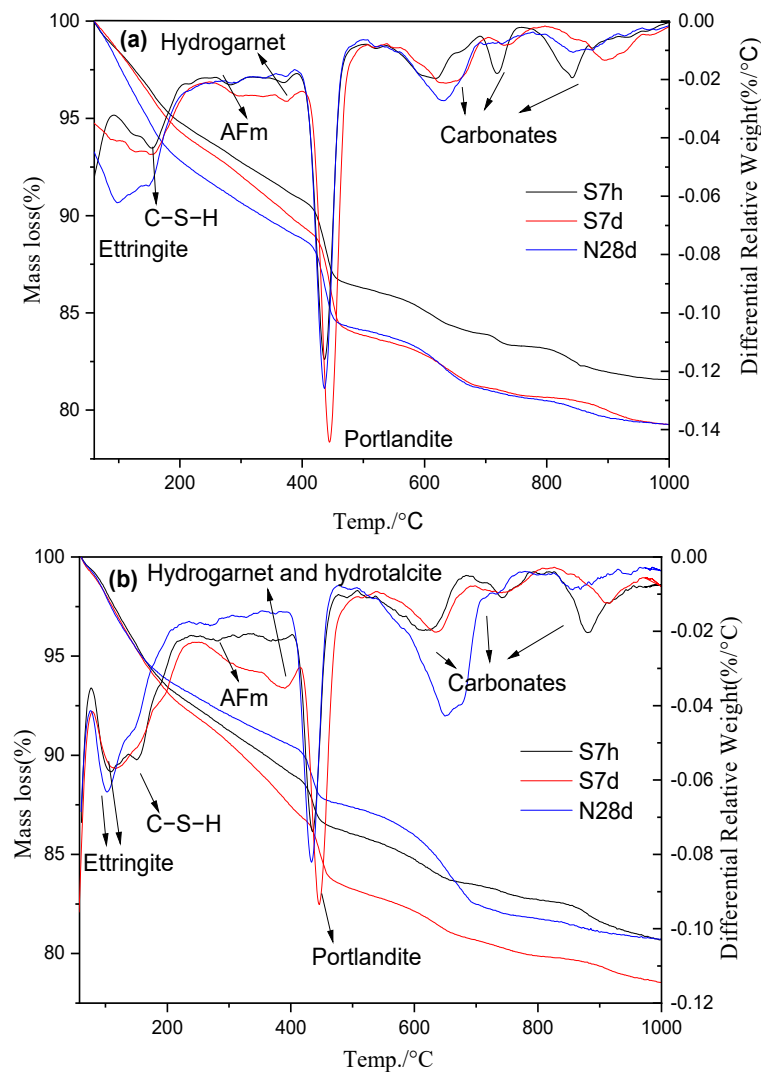


**Figure 11.** TG / DTG curves of Ref (a) and G20 (b) under different curing conditions.

### 3.4. Mechanical Property

The strengths of GBFS-blended cement mortar and pure cement mortar under various curing conditions are shown in Figure 12. It can be seen that the compressive strength of G20 mortar under three curing conditions were all lower than that of Ref mortar. The strength activity index (the strength ratio of G20 mortar to Ref mortar under the same curing condition) under various curing conditions was 92.6%, 82.0%, and 99.7%, respectively, while the corresponding flexural strength activity index was 103.1%, 81.9%, and 109.1%, separately. Despite the fact that the compressive strength activity index of S7h G20 mortar was lower than that of N28d, the difference was slight, indicating that early steam curing improves the hydration activity of GBFS, which is in good agreement with the result of non-evaporable water in Table 3. Although the non-evaporable water in S7d G20 is higher than that of S7d Ref (Table 3), the strength of G20 mortar was much lower than Ref, regardless of compressive strength or flexural strength. This may be related to the formation of a large number of hydrogarnet and more micro-cracks produced in GBFS-blended cement mortar during long-term steam curing (Figure 8e). It should be noted that, compared with compressive strength, flexural strength is more sensitive to cracks; therefore, although the compressive strength of G20 in S7d is higher than that in S7h, the flexural strength of G20 in S7d is less than that in S7h.

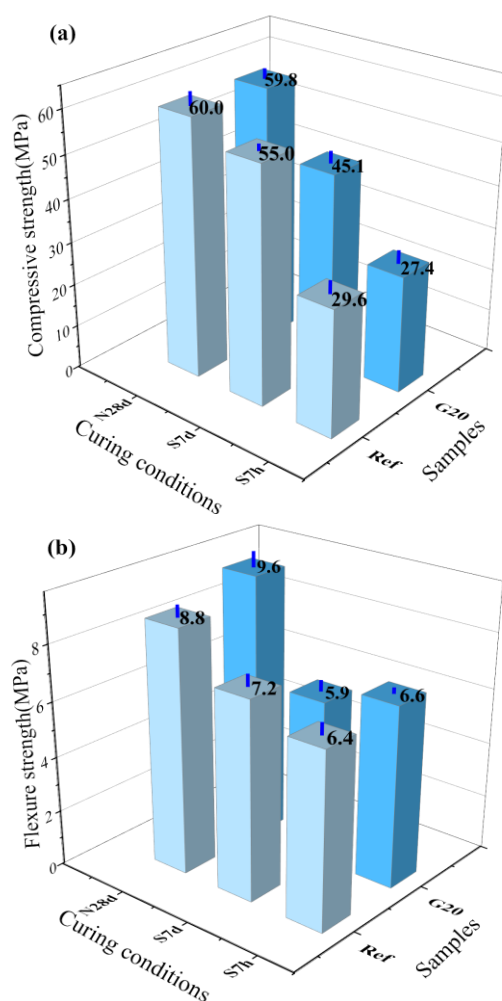


**Figure 12.** Strength of GBFS blended cement mortars, (a) compressive strength, (b) flexural strength.

Under the condition of standard curing for 28 d, G20 has the highest strength activity index including compressive strength and flexural strength, which is related to both the high content of non-evaporable water (Table 3) and its improved dense microstructure, as shown in Figure 10f. In addition, the G20 mortar has a high flexural strength under the conditions of S7h and N28d, which is attributed to the lower CH content, smaller crystal size of CH (Table 3 and Figure 10a) and the improved adherence at the aggregate-paste interface [30].

#### 4. Discussion

The abundant amorphous phase content and the high specific surface area guarantee the high reactivity of GBFS; therefore, besides the filler effects, GBFS can also participate in cement hydration during 80 °C steam curing for 7 h. The presence of a high content of available  $\text{Al}_2\text{O}_3$  and MgO not only changes the composition, but also changes the morphology of hydration products, so that hydrotalcite and the foil-like C-S-H gels were formed. Hydrotalcite can not only consolidate chloride ions, but also can consume the available Al phase required by ettringite formation during the ingress of sulfate; therefore, it is helpful to improve the durability of concrete [31,32]. In addition, a large amount of  $\text{Al}_2\text{O}_3$  in GBFS will inevitably take part in the precipitation of C-S-H gels and form C-(A)-S-H gels under the condition of steam curing, so as to avoid being further sulfate attacked; therefore, the formation of C-(A)-S-H gels is also conducive to the improvement of sulfate resistance [15]. In addition, although the non-evaporable water of G20 under the conditions of S7h and N28d are basically the same, the strength of S7h G20 is much lower than N28d G20 due to the existence of pores under steam curing condition (Figure 6g).

Although the prolongation of steam curing time can improve the non-evaporable water, it also brings the risk of hydrogarnet ( $C_3ASH_4$ ) formation, especially for the cement paste mixed with GBFS. Due to the large amount of available Al phase in GBFS, there is a high probability of aluminate hydrate formation which can be further converted to hydrogarnet in GBFS-mixed cement paste at elevated temperature. It is reported that hydrogarnet formation will cause the reduction of solid phase volume and increase the porosity of concrete [33], which is harmful to the strength improvement and durability of concrete. Accordingly, even though the hydration products of S7d G20 is more abundant (Table 3), its strength is still much lower than that of S7d Ref. Moreover, prolonging the steam curing time will also lead to the increase of cracks and is not conducive to the durability of concrete. Since the formation of hydrotalcite and hydrogarnet can consume the available Al, steam curing for 7 d seems to be more conducive to the formation of C-(A)-S-H with lower Al content than steam curing for 7 h in GBFS-blended cement paste [41].

Under standard curing for 28 d, the structure of G20 is denser and its strength is basically the same as that of Ref, due to both the pozzolanic effect and filler effect of GBFS. In addition, it is worth noting that GBFS incorporation can not only reduce the amount of CH, but also reduce the particle size of CH, so as to improve the structure of the interfacial transition zone and improve the flexural strength of G20 cured under both S7h and N28 conditions.

## 5. Conclusions

This study investigated the influence of GBFS with high content  $Al_2O_3$  and MgO on the early age hydration products and mechanical properties of steam-cured concrete. The hydration products and mechanical properties of cement paste blended with GBFS (0% and 20% replacement) were studied under steam curing conditions (80 °C for 7 h and 7 d) in comparison with standard curing conditions for 28 d. According to the above results, the conclusions are as follows:

- (1) GBFS addition promotes the formation of flake-like hydrotalcite and foil-shaped, equant grain-shaped C-S-H gels, of which hydrotalcite helps to improve the durability of concrete. However, extending the steam curing time to 7 days, more hydrogarnet with larger sizes are further formed due to the higher content of available Al in the GBFS. The generation of hydrogarnet will induce the formation of cracks and increase the porosity, which is detrimental to strength development and durability of concrete.
- (2) The enhanced uptake of Al by C-S-H gels in GBFS-blended cement paste under steam curing promotes the formation of C-(A)-S-H gels, and thereby reduces the Al phase that can react with sulfate under sulfate attack, which is helpful to improve the sulfate resistance of concrete. However, since the formation of hydrotalcite and hydrogarnet reduces the available Al, the prolongation of steam curing time (to 7 d) seems to be more conducive to the formation of low Al C-(A)-S-H gels.
- (3) The non-evaporable water and CH content of GBFS-blended cement paste are basically the same under 80 °C steam curing for 7 h and standard curing for 28 d, indicating that steam curing can significantly accelerate the interaction between cement and GBFS. Under the above three curing conditions, the compressive strength of G20 mortar is 92.6%, 82.0%, and 99.7% that of pure PC mortar, respectively, while the corresponding values for flexural strength are 103.1%, 81.9%, and 109.1%, separately. This indicates that 20% GBFS addition has almost no negative effect on the demolding strength under initial 80 °C steam curing for 7 h; however, extending the steam curing time to 7 d increases the strength gap between 20% GBFS-blended cement mortar and pure cement mortar, which is related to the formation of hydrogarnet and cracks.

**Author Contributions:** B.L.: conceptualization, data curation, investigation, methodology, validation, visualization, writing—original draft, writing—review & editing. Z.T.: data curation, software, investigation, writing—original draft, writing—review & editing. B.H.: formal analysis, investigation, validation, writing—original draft. Z.L.: formal analysis, methodology, validation, writing—review

& editing. Y.C.: formal analysis, methodology, validation, writing—original draft. B.D.: funding acquisition, investigation, resources, writing—original draft. P.Z. formal analysis, funding acquisition, supervision, visualization, writing—review & editing. All authors have read and agreed to the published version of the manuscript.

**Funding:** This research was funded by the Jiangsu Natural Science Foundation (BK20181061), the National Natural Science Foundation of China (No. 11902123, 51778132), Jiangsu Province Construction System Science and Technology Project (No. 2020ZD85, 2021ZD74, 2022ZD100) and the Huai Shang Ying Cai Project.

**Institutional Review Board Statement:** Not applicable.

**Informed Consent Statement:** Not applicable.

**Data Availability Statement:** All data generated or used during the study appear in the submitted article.

**Acknowledgments:** The authors would like to acknowledge the funding support from the Jiangsu Natural Science Foundation, the National Natural Science Foundation of China and Jiangsu Province Construction System Science and Technology Project, and thanks the support from the Huai Shang Ying Cai Project.

**Conflicts of Interest:** The authors declare no conflict of interest.

## References

- Cassagnabère, F.; Mouret, M.; Escadeillas, G. Early hydration of clinker–slag–metakaolin combination in steam curing conditions, relation with mechanical properties. *Cem. Concr. Res.* **2009**, *39*, 1164–1173. [\[CrossRef\]](#)
- Kurpinska, M.; Grzyl, B.; Kristowski, A. Cost Analysis of Prefabricated Elements of the Ordinary and Lightweight Concrete Walls in Residential Construction. *Materials* **2019**, *12*, 3629. [\[CrossRef\]](#)
- Aldea, C.-M.; Young, F.; Wang, K.; Shah, S.P. Effects of curing conditions on properties of concrete using slag replacement. *Cem. Concr. Res.* **2000**, *30*, 465–472. [\[CrossRef\]](#)
- Ramezaniapour, A.; Esmaeili, K.; Ghahari, S.A. Influence of initial steam curing and different types of mineral additives on mechanical and durability properties of self-compacting concrete. *Constr. Build. Mater.* **2014**, *73*, 187–194. [\[CrossRef\]](#)
- Lothenbach, B.; Winnefeld, F.; Alder, C.; Wieland, E.; Lunk, P. Effect of temperature on the pore solution, microstructure and hydration products of Portland cement pastes. *Cem. Concr. Res.* **2007**, *37*, 483–491. [\[CrossRef\]](#)
- Shi, J.; Liu, B.; Wu, X.; Tan, J.; Dai, J.; Ji, R. Effect of steam curing on surface permeability of concrete: Multiple transmission media. *J. Build. Eng.* **2020**, *32*, 101475. [\[CrossRef\]](#)
- Hooton, R.D.; Titherington, M. Chloride resistance of high-performance concretes subjected to accelerated curing. *Cem. Concr. Res.* **2004**, *34*, 1561–1567. [\[CrossRef\]](#)
- Prem, P.R.; Bharatkumar, B.H.; Iyer, N.R. Influence of curing regimes on compressive strength of ultra high performance concrete. *Sadhana* **2013**, *38*, 1421–1431. [\[CrossRef\]](#)
- Liu, B.; Jiang, J.; Shen, S.; Zhou, F.; Shi, J.; He, Z. Effects of curing methods of concrete after steam curing on mechanical strength and permeability. *Constr. Build. Mater.* **2020**, *256*, 119441. [\[CrossRef\]](#)
- Escalante-García, J.; Sharp, J. Effect of temperature on the hydration of the main clinker phases in portland cements: Part ii, blended cements. *Cem. Concr. Res.* **1998**, *28*, 1259–1274. [\[CrossRef\]](#)
- Wang, P.; Fu, H.; Guo, T.; Zuo, W.; Zhao, H.; Tian, L.; Chen, C. Volume deformation of steam-cured concrete with fly ash during and after steam curing. *Constr. Build. Mater.* **2021**, *306*, 124854. [\[CrossRef\]](#)
- Chen, L.; Zheng, K.; Xia, T.; Long, G. Mechanical property, sorptivity and microstructure of steam-cured concrete incorporated with the combination of metakaolin-limestone. *Case Stud. Constr. Mater.* **2019**, *11*, e00267. [\[CrossRef\]](#)
- Liu, J.; Wang, D. The Role of Phosphorus Slag in Steam-Cured Concrete. *Adv. Mater. Sci. Eng.* **2017**, *2017*, 8392435. [\[CrossRef\]](#)
- Li, B.; Cao, R.; You, N.; Chen, C.; Zhang, Y. Products and properties of steam cured cement mortar containing lithium slag under partial immersion in sulfate solution. *Constr. Build. Mater.* **2019**, *220*, 596–606. [\[CrossRef\]](#)
- Li, B.; Huo, B.; Cao, R.; Wang, S.; Zhang, Y. Sulfate resistance of steam cured ferronickel slag blended cement mortar. *Cem. Concr. Compos.* **2019**, *96*, 204–211. [\[CrossRef\]](#)
- Li, B.; Wang, Y.; Yang, L.; Zhang, Y. Sulfate resistance and hydration products of steam cured steel slag blended cement mortar under dry–wet cycle. *J. Sustain. Cem. Mater.* **2019**, *8*, 353–366. [\[CrossRef\]](#)
- Ho, D.W.S.; Chua, C.W.; Tam, C.T. Steam-cured concrete incorporating mineral admixtures. *Cem. Concr. Res.* **2003**, *33*, 595–601. [\[CrossRef\]](#)
- Jung, W.; Choi, S.-J. Effect of High-Temperature Curing Methods on the Compressive Strength Development of Concrete Containing High Volumes of Ground Granulated Blast-Furnace Slag. *Adv. Mater. Sci. Eng.* **2017**, *2017*, 7210591. [\[CrossRef\]](#)
- Gonzalez-Corominas, A.; Etxeberria, M.; Poon, C.S. Influence of steam curing on the pore structures and mechanical properties of fly-ash high performance concrete prepared with recycled aggregates. *Cem. Concr. Compos.* **2016**, *71*, 77–84. [\[CrossRef\]](#)



20. Kolani, B.; Lacarrière, L.; Sellier, A.; Escadeillas, G.; Boutillon, L.; Linger, L. Hydration of slag-blended cements. *Cem. Concr. Compos.* **2012**, *34*, 1009–1018. [[CrossRef](#)]
21. Barnett, S.; Soutsos, M.; Millard, S.; Bungey, J. Strength development of mortars containing ground granulated blast-furnace slag: Effect of curing temperature and determination of apparent activation energies. *Cem. Concr. Res.* **2006**, *36*, 434–440. [[CrossRef](#)]
22. Yu, Y.; Jin, Z.; Shao, S.; Zhang, X.; Li, N.; Xiong, C. Evolution of temperature stress and tensile properties of concrete during steam-curing process. *Constr. Build. Mater.* **2020**, *256*, 119441. [[CrossRef](#)]
23. Shiyu, Z.; Qiang, W.; Yuqi, Z. Research on the resistance to saline soil erosion of high-volume mineral admixture steam-cured concrete. *Constr. Build. Mater.* **2019**, *202*, 1–10. [[CrossRef](#)]
24. Kucharczyk, S.; Zajac, M.; Stabler, C.; Thomsen, R.M.; Ben Haha, M.; Skibsted, J.; Deja, J. Structure and reactivity of synthetic CaO-Al<sub>2</sub>O<sub>3</sub>-SiO<sub>2</sub> glasses. *Cem. Concr. Res.* **2019**, *120*, 77–91. [[CrossRef](#)]
25. Ahmad, J.; Kontoleon, K.J.; Majdi, A.; Naqash, M.T.; Deifalla, A.F.; Ben Kahla, N.; Isleem, H.F.; Qaidi, S.M.A. A Comprehensive Review on the Ground Granulated Blast Furnace Slag (GGBS) in Concrete Production. *Sustainability* **2022**, *14*, 8783. [[CrossRef](#)]
26. Li, L.; Feng, J.; Lu, Z.; Xie, H.; Xiao, B.; Kwan, A.; Jiao, C. Effects of aggregate bulking and film thicknesses on water permeability and strength of pervious concrete. *Powder Technol.* **2022**, *396*, 743–753. [[CrossRef](#)]
27. Chen, W.; Brouwers, H.J.H. The hydration of slag, part 2: Reaction models for blended cement. *J. Mater. Sci.* **2006**, *42*, 444–464. [[CrossRef](#)]
28. Bougara, A.; Lynsdale, C.; Milestone, N. Reactivity and performance of blastfurnace slags of differing origin. *Cem. Concr. Compos.* **2010**, *32*, 319–324. [[CrossRef](#)]
29. Escalante, J.; Gómez, L.; Johal, K.; Mendoza, G.; Mancha, H.; Méndez, J. Reactivity of blast-furnace slag in Portland cement blends hydrated under different conditions. *Cem. Concr. Res.* **2001**, *31*, 1403–1409. [[CrossRef](#)]
30. Özbay, E.; Erdemir, M.; Durmuş, H.I. Utilization and efficiency of ground granulated blast furnace slag on concrete properties—A review. *Constr. Build. Mater.* **2016**, *105*, 423–434. [[CrossRef](#)]
31. Yang, Z.; Fischer, H.; Polder, R. Modified hydrotalcites as a new emerging class of smart additive of reinforced concrete for anticorrosion applications: A literature review. *Mater. Corros.* **2013**, *64*, 1066–1074. [[CrossRef](#)]
32. Yan, X.; Jiang, L.; Guo, M.; Chen, Y.; Song, Z.; Bian, R. Evaluation of sulfate resistance of slag contained concrete under steam curing. *Constr. Build. Mater.* **2019**, *195*, 231–237. [[CrossRef](#)]
33. Quillin, K.; Osborne, G.; Majumdar, A.; Singh, B. Effects of w/c ratio and curing conditions on strength development in BRECEM concretes. *Cem. Concr. Res.* **2001**, *31*, 627–632. [[CrossRef](#)]
34. Jappy, T.G.; Glasser, F.P. Synthesis and stability of silica-substituted hydrogarnet Ca<sub>3</sub>Al<sub>2</sub>Si<sub>3-x</sub>O<sub>12-4x</sub>(OH)<sub>4x</sub>. *Adv. Cem. Res.* **1991**, *4*, 1–8. [[CrossRef](#)]
35. Fu, Y.; Ding, J.; Beaudoin, J. Zeolite-based additives for high alumina cement products. *Adv. Cem. Based Mater.* **1996**, *3*, 37–42. [[CrossRef](#)]
36. Sha, W. Differential scanning calorimetry study of the hydration products in portland cement pastes with metakaolin replacement. *Adv. Build. Technol.* **2002**, *1*, 881–888. [[CrossRef](#)]
37. Song, S.; Sohn, D.; Jennings, H.M.; Mason, T.O. Hydration of alkali-activated ground granulated blast furnace slag. *J. Mater. Sci.* **2000**, *35*, 249–257. [[CrossRef](#)]
38. Bernard, E.; Lothenbach, B.; Cau-Dit-Coumes, C.; Chlique, C.; Dauzères, A.; Pochard, I. Magnesium and calcium silicate hydrates, Part I: Investigation of the possible magnesium incorporation in calcium silicate hydrate (C-S-H) and of the calcium in magnesium silicate hydrate (M-S-H). *Appl. Geochem.* **2018**, *89*, 229–242. [[CrossRef](#)]
39. Ríos, C.; Williams, C.; Fullen, M. Hydrothermal synthesis of hydrogarnet and tobermorite at 175 °C from kaolinite and metakaolinite in the CaO–Al<sub>2</sub>O<sub>3</sub>–SiO<sub>2</sub>–H<sub>2</sub>O system: A comparative study. *Appl. Clay Sci.* **2009**, *43*, 228–237. [[CrossRef](#)]
40. Walkley, B.; Nicolas, R.S.; Sani, M.-A.; Bernal, S.A.; van Deventer, J.S.; Provis, J.L. Structural evolution of synthetic alkali-activated CaO-MgO-Na<sub>2</sub>O-Al<sub>2</sub>O<sub>3</sub>-SiO<sub>2</sub> materials is influenced by Mg content. *Cem. Concr. Res.* **2017**, *99*, 155–171. [[CrossRef](#)]
41. Liu, L.; Sun, C.; Geng, G.; Feng, P.; Li, J.; Dähn, R. Influence of decalcification on structural and mechanical properties of synthetic calcium silicate hydrate (C-S-H). *Cem. Concr. Res.* **2019**, *123*, 105793. [[CrossRef](#)]
42. Kunther, W.; Ferreiro, S.; Skibsted, J. Influence of the Ca/Si ratio on the compressive strength of cementitious calcium–silicate–hydrate binders. *J. Mater. Chem. A* **2017**, *5*, 17401–17412. [[CrossRef](#)]
43. Manoli, F.; Dalas, E. Spontaneous precipitation of calcium carbonate in the presence of ethanol, isopropanol and diethylene glycol. *J. Cryst. Growth* **2000**, *218*, 359–364. [[CrossRef](#)]
44. Durdziński, P.T. *Hydration of Multi-Component Cements Containing Cement Clinker, Slag, Calcareous Fly Ash and Limestone*; EPFL: Lausanne, Switzerland, 2016. [[CrossRef](#)]
45. Liu, B.; Xie, Y.; Li, J. Influence of steam curing on the compressive strength of concrete containing supplementary cementing materials. *Cem. Concr. Res.* **2005**, *35*, 994–998. [[CrossRef](#)]